Published in final edited form as:
Science. 2013 July 5; 341(6141): . doi:10.1126/science.1238856.

Engineered SIRPα variants as immunotherapeutic adjuvants to anti-cancer antibodies

Kipp Weiskopf[1,2,†], **Aaron M. Ring**[1,2,3,4,†], **Chia Chi M. Ho**[1,2,3,4], **Jens-Peter Volkmer**[1,2], **Aron M. Levin**[3,4], **Anne Kathrin Volkmer**[1,2,5], **Engin Özkan**[3,4], **Nathaniel B. Fernhoff**[1,2], **Matt van de Rijn**[6], **Irving L. Weissman**[1,2,6], and **K. Christopher Garcia**[3,4,*]

[1]Institute for Stem Cell Biology and Regenerative Medicine, and the Ludwig Center for Cancer Stem Cell Research and Medicine, Stanford University School of Medicine, Stanford, California 94305, USA

[2]Stanford Cancer Institute, Stanford University School of Medicine, Stanford, California 94305, USA

[3]Department of Molecular and Cellular Physiology, and Department of Structural Biology, Stanford University School of Medicine, Stanford, California 94305, USA

[4]Howard Hughes Medical Institute, Stanford University School of Medicine, Stanford, California 94305, USA

[5]Department of Obstetrics and Gynaecology, University of Dusseldorf, Germany

[6]Department of Pathology, Stanford University Medical Center, Stanford, California 94305, USA

Abstract

During oncogenesis, tumors develop mechanisms to avoid rejection by the immune system. Recent studies have identified CD47 as an anti-phagocytic “don't eat me” signal tat cancer cells employ to inhibit macrophage-mediated destruction. Here, we modified the 14 kDa binding domain of human SIRPα, the receptor for CD47, for use as a CD47 antagonist. Using *in vitro* evolution via yeast surface display, we engineered high-affinity SIRPα variants with up to a 50,000-fold increase in affinity for human CD47 relative to wild-type SIRPα. As high-affinity SIRPα monomers, the variants potently antagonized CD47 on cancer cells, but to our surprise, they did not induce macrophage phagocytosis on their own. Instead, the high-affinity SIRPα monomers exhibited remarkable synergy with all tumor-specific monoclonal antibodies tested by increasing phagocytosis *in vitro* and enhancing anti-tumor responses *in vivo*. This novel “one-two punch” directs immune responses against tumor cells while lowering the threshold for macrophage activation, thereby providing a universal method for augmenting the efficacy of therapeutic anti-cancer antibodies.

*Correspondence to: kcgarcia@stanford.edu.
†These authors contributed equally to this work.

Author contributions: K.W. and A.M.R conceived of engineering high-affinity SIRPα variants, designed all experiments, and wrote the manuscript. A.M.R., C.C.M.H, and A.M.L. performed directed evolution of the high-affinity SIRPα variants with yeast display. K.W. and A.M.R. further engineered the CV1 variant and SIRPα-Fc fusions proteins. A.M.R. and C.C.M.H conducted SPR affinity measurements. A.M.R. crystallized the FD6:CD47 complex, and A.M.R. and E.Ö. determined and refined the structure. K.W. and A.M.R. prepared proteins for functional and *in vivo* studies. K.W. and A.M.R. performed binding/blocking assays on cancer cells. K.W. performed *in vitro* phagocytosis experiments. K.W., J.P.V., A.V., and N.B.F. performed *in vivo* experiments. M.v.d.R. performed pathological analysis. I.L.W. and K.C.G. supervised the research and edited the manuscript.

Supplementary Materials: Materials and Methods
Figures S1-S14
Tables S1
Movies S1-S2

The ability of tumors to evade the immune system is an emerging hallmark of cancer (1), and new therapeutic strategies that direct immune responses against cancer cells show promise in experimental and clinical settings (2, 3). Macrophages commonly infiltrate tumors and their tumoricidal potential can be harnessed to benefit patients (4). Recent studies have identified CD47 as an anti-phagocytic “don't eat me” signal that distinguishes live cells from dying or aged cells (5, 6), and CD47 is highly expressed by many types of cancer to avoid detection by macrophages (7-11). CD47 expression also limits Fc receptor-mediated phagocytosis in response to therapeutic antibodies (9). Antibodies that block binding of CD47 to SIRPα, an inhibitory receptor expressed on macrophages, greatly increase phagocytosis of cancer cells (8-11). However, antibodies have limited tissue distribution and can exert off-target effects due to Fc-mediated functions (12, 13). In this study, we aimed to improve CD47-targeted therapies by utilizing the single 14 kDa binding domain of human SIRPα as a competitive antagonist to human CD47 (Fig. 1A). Due to the weak ~1 μM affinity of the native SIRPα-CD47 interaction (14-16), we found that wild-type SIRPα was a poor antagonist which precluded its use as a potential therapeutic. Therefore, we exploited structural knowledge of the CD47-SIRPα interaction and performed *in vitro* evolution via yeast surface display to engineer high-affinity SIRPα variants that would act as potent CD47 antagonists.

To improve the affinity of human SIRPα for human CD47, we created mutant libraries of the N-terminal V-set Ig domain of SIRPα (residues 1-118) conjugated to Aga2p for yeast surface-display (schematized in Fig. 1B). Using the CD47 IgSF domain as a selection reagent, we conducted two ‘generations’ of *in vitro* evolution. The first generation entailed five rounds of selection from a pooled mutant library containing randomizations to two classes of SIRPα residues—those that contact CD47 or those that reside within the hydrophobic core (Fig. S1A) (15, 16). The resulting first generation SIRPα variants bound CD47 with 20-100-fold higher affinity than wild-type SIRPα as measured by surface plasmon resonance (Fig. 1C; clones 1D4 and 1A5, Fig. S1B). To obtain even higher-affinity variants, we performed a second generation of directed evolution by constructing a library that achieved full-coverage of thirteen residues mutated in the first generation selectants (Fig. S2). After five additional rounds of selection, we obtained variants that bound CD47 with dissociation constants (K_D) as low as 34.0 pM and dissociation half-lives ($t_{1/2}$) as long as 44 minutes compared to 0.3-0.5 μM K_D and 1.8 seconds $t_{1/2}$ for wild-type SIRPα (Fig. 1C; clones 2D3 through FA4). Interestingly, the sequences of the high-affinity SIRPα variants converged on a consensus set of mutations. When we grafted these nine conservative substitutions onto the predominant wild-type human SIRPα allele (17) (allele 2), the resulting variant (termed CV1, consensus variant 1) bound human CD47 with an affinity of 11.1 pM (Fig. 1C).

To understand whether the high-affinity SIRPα variants retained a CD47-binding geometry similar to the wild-type protein, we determined the crystal structure of a complex between the high-affinity variant FD6 and the human CD47 IgSF domain (Fig. 1D, Fig. S3, and Table S1). The FD6:CD47 complex superimposed with the wild-type SIRPα:CD47 complex (15) with a root mean square deviation of only 0.61 Å, indicating a high degree of structural similarity and validating our efforts to preserve the geometry of the wild-type interaction (Fig. 1E). The overlapping binding modes of FD6 and wild-type SIRPα for CD47 indicate they would compete for the same CD47 epitope, thereby providing maximal potential antagonism. As a notable difference, the C′D loop of FD6 contains three of the four contact mutations present in the consensus sequence (Fig. 1E, lower inset). We speculate these mutations stabilize the C′D loop, which positions the positive charge of Arg53 into a cluster of glutamic acids on CD47 (Fig. 1E, lower inset). The remainder of the binding interface between FD6 and CD47 highly resembles the wild-type SIRPα:CD47 interface, with the

most notable exception being the mutation of Ile31 to Phe (Fig. 1E, upper inset). Therefore, these structural studies imply the high-affinity SIRPα variants could serve as efficacious CD47 antagonists.

We examined the functional properties of the high-affinity SIRPα variants by assessing their ability to bind and antagonize CD47 on the surface of human cancer cells. We found that SIRPα variants with increased CD47 affinity exhibited greater potency in binding (Fig. S4A and C) and blocking cell-surface CD47 (Fig. 2A and Fig. S4B). As single-domain monomers (Fig. S5A), both FD6 and CV1 variants exhibited potent antagonism relative to wild-type SIRPα. Importantly, both high-affinity variants were more potent CD47 antagonists than Fab fragments produced from anti-CD47 antibody clone B6H12, a well-characterized CD47 antagonist that demonstrates therapeutic efficacy *in vitro* and *in vivo* (Fig. 2A) (8-11).

We next evaluated the ability of high-affinity SIRPα variants to increase phagocytosis *in vitro* by co-culturing macrophages and tumor cells in the presence of CD47 blocking agents. As fusion proteins to the Fc fragment of human IgG4 (hIgG4; Fig. S5A), the high-affinity SIRPα variants led to dramatic increases in phagocytosis of cancer cells as visualized by microscopy (Fig. 2B, Movies S1 and S2). To obtain quantitative measurements of phagocytosis, primary human macrophages and GFP^+ tumor cells were co-cultured with CD47-blocking agents and the percentage of macrophages that became GFP^+ was analyzed by flow cytometry (Fig. 2C and Fig. S6). Using multiple human cancer cell lines representing both solid and hematologic malignancies, we found that treatment with saturating concentrations of high-affinity SIRPα-hIgG4 variants produced dramatic increases in phagocytosis relative to wild-type SIRPα-hIgG4 controls (Fig. 2D). To our surprise, no substantial levels of phagocytosis were observed upon treatment with high-affinity SIRPα monomers or B6H12 Fab fragments at concentrations that maximally antagonize CD47 (Fig. 2D and Fig. S5C). Similarly, high-affinity SIRPα dimers produced without Fc chains failed to induce phagocytosis, excluding CD47 oligomerization as a mechanism of action for the SIRPα-hIgG4 fusions (Fig. S5D). These findings demonstrate that blocking CD47 alone does not induce phagocytosis. Instead, phagocytosis was only observed when CD47 was blocked in the presence of antibody Fc chains, which contribute a pro-phagocytic stimulus.

Consequently, we hypothesized that treatment with high-affinity SIRPα monomers would enhance phagocytosis in the presence of tumor-specific monoclonal antibodies. To investigate this hypothesis, we performed phagocytosis assays using antibodies targeting DLD-1 cells, a human colon cancer cell line. When high-affinity SIRPα monomers were added alone or in combination with a non-specific isotype control antibody, basal levels of phagocytosis were observed (Fig. 2E). Treatment with either anti-CD47 clone 2D3, which binds CD47 but does not block the interaction with SIRPα (18), or an anti-EpCam antibody produced moderate levels of phagocytosis. As a proof-of-concept, addition of high-affinity SIRPα monomer FD6 to both antibody treatments resulted in significant increases in phagocytosis (Fig. 2E).

To demonstrate the clinical implications of this principle, we examined the ability of high-affinity SIRPα monomers to enhance the efficacy of established monoclonal antibodies currently used as cancer therapies. First, phagocytosis assays were performed using the $Her2/neu^+$ breast cancer cell line SK-BR-3 (19). Basal levels of phagocytosis were observed upon treatment with vehicle or SIRPα monomers alone, while treatment with the therapeutic anti-Her2/neu antibody trastuzumab led to moderate increases in phagocytosis (Fig. 2F). No further increase in phagocytosis was observed upon addition of wild-type SIRPα monomer to trastuzumab. However, the combination of trastuzumab with high-affinity SIRPα

monomers FD6 or CV1—which potently block CD47—resulted in maximal levels of phagocytosis that were considerably higher than the additive effect of either agent administered alone.

Next, we tested the high-affinity SIRPα monomers for synergy with the anti-EGFR antibody cetuximab using DLD-1 colon cancer cells. Phagocytosis was evaluated in response to varying concentrations of cetuximab alone, in combination with wild-type SIRPα monomer, or in combination with high-affinity SIRPα monomers. Relative to both cetuximab alone or with wild-type SIRPα monomer, the addition of high-affinity SIRPα monomers to cetuximab resulted in a significant increase in both the maximal efficacy and potency of the therapeutic antibody (Fig. 2G). Similar effects were observed when phagocytosis was evaluated with Raji lymphoma cells treated with varying concentrations of rituximab, an anti-CD20 antibody (Fig. 2H). Again, high-affinity SIRPα monomers increased both the maximal efficacy and potency of rituximab. For both antibodies, the left-shift in the concentration-response curves upon addition of high-affinity SIRPα monomers demonstrates that CD47 blockade lowers the threshold for macrophage phagocytosis. Using a panel of recombinant anti-CD20 antibodies that contain the rituximab variable region and differing heavy chain isotypes, we found that CV1 monomer was able to augment phagocytosis in response to all human IgG subclasses (Fig. S7). Therefore, the high-affinity SIRPα monomers could act as universal adjuvants to tumor-specific antibodies.

We next evaluated these principles *in vivo* by investigating the activity of the high-affinity SIRPα variants in mouse tumor models. We engrafted human tumors into NSG (NOD scid gamma) mice, which lack functional T, B, and NK cells but retain functional macrophages (9, 10, 20). Importantly, NSG mice also express a SIRPα allele that binds human CD47 and inhibits macrophage activity, thereby enabling *in vivo* evaluation of human CD47 blockade (9, 10, 17, 21, 22). As a proof-of-concept study, we tested CV1-hIgG4 in a model of human bladder cancer to demonstrate a single molecule that combines a high-affinity SIRPα domain with a pro-phagocytic signal can exhibit efficacy as a single agent. GFP-luciferase^{+} 639-V bladder cancer cells were injected into the dorsal subcutaneous tissue of NSG mice. Engraftment was confirmed by bioluminescence imaging and mice were randomized into groups for daily treatment with vehicle control or approximately 7.5 mg/kg CV1-hIgG4. Treatment with CV1-hIgG4 substantially reduced tumor growth rates as evaluated by bioluminescence imaging (Fig. 3A and B). Accordingly, a significant benefit in survival was observed even after discontinuing treatment once all control mice had died (Fig. 3C). In CV1-hIgG4 treated mice, palpable stromal tissue developed around the sites of tumor engraftment. Histological examination of this tissue revealed small tumor nodules embedded in an extensive inflammatory infiltrate containing macrophages with evidence of phagocytosis (Fig. S8A-C).

Previous xenograft studies examining anti-CD47 therapies used reagents that exclusively targeted human CD47 and did not bind mouse CD47 (8-11, 23). Although wild-type human SIRPα does not bind mouse CD47, the high-affinity SIRPα variants acquired cross-reactivity with mouse CD47 (Fig. S9). Thus, our *in vivo* models allow for evaluation of efficacy in the presence of a large ‘antigen sink’ and toxicity due to CD47 expression on normal mouse cells. Examination of the blood of treated animals revealed that CV1-hIgG4 coated all mouse blood cells (Fig. 3D) and resulted in the development of chronic anemia as a side effect of therapy (Fig. 3E). No toxicity to other blood lineages was observed (Fig. S8D). Red blood cell loss has also been observed with anti-mouse CD47 antibodies (10), consistent with our findings here.

We further examined the safety of the high-affinity SIRPα variants in a toxicity study with cynomolgus macaques, which express a CD47 orthologue that is nearly identical to human

CD47 (Fig. S10A and B). A single low-dose (1.5 mg/kg) injection of high-affinity SIRPα-Fc into two independent animals produced a substantial drop in red blood cells (Fig. 3F), similar to our findings in mice. By contrast, no hematologic toxicity was observed in an animal treated with a dose escalation of high-affinity SIRPα monomer from 0.3 mg/kg to 10 mg/kg. No toxicity to other blood lineages or organ systems was detected in any of the animals, nor did we detect evidence of anaphylactic reactions (Fig. S10C and D). These findings further demonstrate that a single molecule that blocks CD47 and contains a pro-phagocytic stimulus, such as antibody Fc chains, produces toxicity. We therefore surmised that the high-affinity SIRPα monomers may offer an alternative and improved strategy for targeting CD47. By using an independent antibody against a tumor antigen, the immune response can be directed specifically against cancer cells. Addition of the high-affinity SIRPα monomers will enhance this immune response while sparing normal cells expressing CD47, as the monomers do not exert significant activity in the absence of Fc. In this manner, the adjuvant approach of the high-affinity monomers enables a wider therapeutic window for immune intervention than other CD47-targeted therapies such as anti-CD47 antibodies or SIRPα-Fc.

To explore the *in vivo* potential of the high-affinity SIRPα monomers, combination with rituximab was evaluated in a localized model of lymphoma. One million GFP-luciferase^{+} Raji cells were subcutaneously engrafted into the flanks of NSG mice. Eight days post-engraftment (Fig. S11A), mice were randomized into groups for a three-week course of daily treatment with either vehicle, CV1 monomer alone, rituximab alone, or a combination of rituximab plus CV1 monomer (approximately 7.5 mg/kg for each therapy). Treatment with CV1 monomer or rituximab alone only slowed tumor growth, whereas the combination therapy completely eliminated tumors in the majority of mice (Fig. 4A-C). During the course of treatment, no toxicity to red blood cells or other hematologic lineages was observed (Fig. S12). The effects of each therapy translated to respective trends in survival curves (Fig. 4D). Remarkably, the synergistic effect of combining a high-affinity SIRPα monomer with a tumor-specific monoclonal antibody led to cures in the majority of animals that persisted long after treatment was discontinued (Fig. 4D and S11B). Similarly, the combination therapy remained effective against large Raji tumors, where significant effects on tumor growth were observed with only a short course of treatment (Fig. S13A and B). These findings validate our strategy as a safe and effective approach to antagonizing CD47 and provide a proof-of-concept demonstration that the high-affinity SIRPα monomers can augment the efficacy of therapeutic antibodies *in vivo*.

To evaluate the therapeutic mechanism of the CV1 monomer/rituximab combination, we performed immunohistochemical staining for macrophages in the large Raji tumors after treatment. Tumors treated with rituximab alone contained moderate levels of macrophages, while treatment with the CV1 monomer/rituximab combination exhibited intense macrophage infiltration as a result of the therapy (Fig. S13C and D). The extent of macrophage infiltration and therapeutic efficacy *in vivo* paralleled the degree of phagocytosis *in vitro* by NSG mouse macrophages (Fig. S13E). Together, these findings indicate that macrophages are effector cells for the CV1 monomer/rituximab therapy, as has previously been confirmed for rituximab and anti-CD47 antibodies (8, 9).

As a demonstration of the general applicability of the high-affinity SIRPα monomers' adjuvant function, we administered the high-affinity SIRPα monomers in combination with alemtuzumab (anti-CD52), a second therapeutic antibody targeting Raji lymphoma cells (24). Localized tumors were allowed to grow for eight days, and mice were randomized into treatment with vehicle control, CV1 monomer alone, alemtuzumab alone, or the combination of CV1 monomer and alemtuzumab. Treatment was given twice per week to evaluate efficacy of the high-affinity SIRPα monomers with less frequent dosing. On this

treatment schedule, CV1 monomer alone produced no significant difference in tumor growth or survival relative to the vehicle control group (Fig. 4E and F). However, addition of CV1 monomer to alemtuzumab resulted in a significant reduction in tumor growth relative to treatment with alemtuzumab alone. Importantly, the combination of alemtuzumab and CV1 monomer substantially prolonged survival and cured 30% of the mice (Fig. S11C), which was a striking improvement from the alemtuzumab alone group in which all mice died during the course of the experiment.

In a third model, Her2/neu$^+$ BT474M1 breast cancer cells were engrafted into the mammary tissue of female NSG mice, and tumors were allowed to grow for two months to approximately 1 cm in diameter (~200 mm^3; Fig. 4G). Mice were randomized into treatment groups with vehicle control, daily administration of CV1 monomer, bi-weekly administration of trastuzumab, or the combination of trastuzumab and CV1 monomer. Treatment with CV1 monomer alone had no effect on tumor growth, while trastuzumab alone was able to reduce tumor volume over time (Fig. 4H). However, the addition of CV1 monomer to the therapeutic antibody regimen enhanced tumor regression (Fig. 4H), consistent with the results observed with rituximab and alemtuzumab.

Monoclonal antibodies are among the most promising agents of targeted cancer therapy. Antibodies have already demonstrated considerable clinical success, but they often elicit limited responses and relapse is common following therapy (25-27). Most studies have focused on identifying new tumor-specific antigens; here, we have developed reagents that enhance the efficacy of tumor-specific antibodies and thus could act as universal adjuvants to monoclonal antibody therapies. Since many cancers overexpress CD47 (8-11), the high-affinity SIRPα variants could be broadly applied as therapeutics. Additionally, as 14 kDa single domains, the high-affinity SIRPα monomers are amenable to further engineering and modifications could be made to alter their efficacy, toxicity, or pharmacokinetic parameters.

Our findings provide further insight into the activity of macrophages against cancer, creating a new model for the action of CD47-targeting therapies (Fig. S14). As observed with high-affinity SIRPα monomers, blockade of CD47 alone does not induce phagocytosis. Similarly, when CD47 is free to transduce inhibitory signals through SIRPα on macrophages, monoclonal antibodies do not achieve their maximal efficacy. However, macrophages are robustly stimulated when CD47 is blocked by high-affinity SIRPα monomers in the presence of surface-bound antibody Fc chains, which stimulate macrophage Fc receptors. High-affinity SIRPα-Fc fusion proteins and anti-CD47 antibodies combine a CD47 blocking component and a pro-phagocytic antibody Fc into a single molecule; hence they exhibit efficacy as single agents but produce toxicity as a trade-off. On the other hand, the combination of high-affinity SIRPα monomers with a separate, anti-tumor monoclonal antibody specifically directs macrophage attack against cancer cells. This strategy offers clear advantages, and with over a hundred antibodies under clinical investigation (28), the number of patients that could benefit from treatment with high-affinity SIRPα monomers will undoubtedly increase. Overall, this study deepens our knowledge of macrophage responses to malignant cells and supports further evaluation of the high-affinity SIRPα reagents as immunotherapies for cancer.

Supplementary Material

Refer to Web version on PubMed Central for supplementary material.

Acknowledgments

The authors wish to thank members of the Weissman and Garcia labs for helpful advice and discussions. The authors thank R. Majeti, J. Liu, and the CD47 Disease Team for discussions and providing anti-CD47 antibodies.

The authors thank T. Storm, L. Jerabek, H. Contreras-Trujillo, A. McCarty, S. Jaiswal, B. di Robilant, S. Varma, T. Naik, S. Willingham, H. Kohrt, N. Goriatcheva, D. Waghray, and S. Fischer for technical assistance, discussions, and reagents. Research reported in this publication was supported by the National Cancer Institute (F30CA168059 to K.W.), the National Institute of Diabetes and Digestive and Kidney Diseases (F30DK094541 to A.M.R.), the Stanford Medical Scientist Training Program (NIH-GM07365 to K.W. and A.M.R.), the Stanford University SPARK Program (to K.W. and A.M.R.), the Deutsche Forschungsgemeinschaft (VO 1976/1 to A.K.V), the Joseph & Laurie Lacob Gynecologic/Ovarian Cancer Fund (to I.L.W), the Virginia and D.K. Ludwig Fund for Cancer Research (to I.L.W), and the Howard Hughes Medical Institute (to K.C.G). The content of this manuscript is solely the responsibility of the authors.

References and Notes

1. Hanahan D, Weinberg RA. Hallmarks of cancer: the next generation. Cell. 2011; 144:646. [PubMed: 21376230]
2. Leach DR, Krummel MF, Allison JP. Enhancement of antitumor immunity by CTLA-4 blockade. Science. 1996; 271:1734. [PubMed: 8596936]
3. Korman AJ, Peggs KS, Allison JP. Checkpoint blockade in cancer immunotherapy. Adv Immunol. 2006; 90:297. [PubMed: 16730267]
4. Beatty GL, et al. CD40 agonists alter tumor stroma and show efficacy against pancreatic carcinoma in mice and humans. Science. 2011; 331:1612. [PubMed: 21436454]
5. Oldenborg PA, et al. Role of CD47 as a marker of self on red blood cells. Science. 2000; 288:2051. [PubMed: 10856220]
6. Gardai SJ, et al. Cell-surface calreticulin initiates clearance of viable or apoptotic cells through trans-activation of LRP on the phagocyte. Cell. 2005; 123:321. [PubMed: 16239148]
7. Jaiswal S, et al. CD47 is upregulated on circulating hematopoietic stem cells and leukemia cells to avoid phagocytosis. Cell. 2009; 138:271. [PubMed: 19632178]
8. Majeti R, et al. CD47 is an adverse prognostic factor and therapeutic antibody target on human acute myeloid leukemia stem cells. Cell. 2009; 138:286. [PubMed: 19632179]
9. Chao MP, et al. Anti-CD47 antibody synergizes with rituximab to promote phagocytosis and eradicate non-Hodgkin lymphoma. Cell. 2010; 142:699. [PubMed: 20813259]
10. Willingham SB, et al. The CD47-signal regulatory protein alpha (SIRPa) interaction is a therapeutic target for human solid tumors. Proc Natl Acad Sci U S A. 2012; 109:6662. [PubMed: 22451913]
11. Edris B, et al. Antibody therapy targeting the CD47 protein is effective in a model of aggressive metastatic leiomyosarcoma. Proc Natl Acad Sci U S A. 2012; 109:6656. [PubMed: 22451919]
12. Beckman RA, Weiner LM, Davis HM. Antibody constructs in cancer therapy: protein engineering strategies to improve exposure in solid tumors. Cancer. 2007; 109:170. [PubMed: 17154393]
13. Tabrizi MA, Roskos LK. Preclinical and clinical safety of monoclonal antibodies. Drug Discov Today. 2007; 12:540. [PubMed: 17631248]
14. Brooke G, Holbrook JD, Brown MH, Barclay AN. Human lymphocytes interact directly with CD47 through a novel member of the signal regulatory protein (SIRP) family. J Immunol. Aug 15.2004 173:2562. [PubMed: 15294972]
15. Hatherley D, et al. Paired receptor specificity explained by structures of signal regulatory proteins alone and complexed with CD47. Mol Cell. 2008; 31:266. [PubMed: 18657508]
16. Hatherley D, Harlos K, Dunlop DC, Stuart DI, Barclay AN. The structure of the macrophage signal regulatory protein alpha (SIRPalpha) inhibitory receptor reveals a binding face reminiscent of that used by T cell receptors. J Biol Chem. 2007; 282:14567. [PubMed: 17369261]
17. Takenaka K, et al. Polymorphism in Sirpa modulates engraftment of human hematopoietic stem cells. Nat Immunol. 2007; 8:1313. [PubMed: 17982459]
18. Seiffert M, et al. Human signal-regulatory protein is expressed on normal, but not on subsets of leukemic myeloid cells and mediates cellular adhesion involving its counterreceptor CD47. Blood. 1999; 94:3633. [PubMed: 10572074]
19. Stancovski I, et al. Mechanistic aspects of the opposing effects of monoclonal antibodies to the ERBB2 receptor on tumor growth. Proc Natl Acad Sci U S A. 1991; 88:8691. [PubMed: 1717984]

20. Shultz LD, et al. Human lymphoid and myeloid cell development in NOD/LtSz-scid IL2R gamma null mice engrafted with mobilized human hemopoietic stem cells. J Immunol. 2005; 174:6477. [PubMed: 15879151]
21. Yamauchi T, et al. Polymorphic Sirpa is the genetic determinant for NOD-based mouse lines to achieve efficient human cell engraftment. Blood. 2013; 121:1316. [PubMed: 23293079]
22. Rodriguez PL, et al. Minimal “Self” peptides that inhibit phagocytic clearance and enhance delivery of nanoparticles. Science. 2013; 339:971. [PubMed: 23430657]
23. Theocharides AP, et al. Disruption of SIRPalpha signaling in macrophages eliminates human acute myeloid leukemia stem cells in xenografts. J Exp Med. 2012; 209:1883. [PubMed: 22945919]
24. Lapalombella R, et al. A novel Raji-Burkitt's lymphoma model for preclinical and mechanistic evaluation of CD52-targeted immunotherapeutic agents. Clin Cancer Res. 2008; 14:569. [PubMed: 18223233]
25. Maloney DG, et al. IDEC-C2B8 (Rituximab) anti-CD20 monoclonal antibody therapy in patients with relapsed low-grade non-Hodgkin's lymphoma. Blood. 1997; 90:2188. [PubMed: 9310469]
26. Vogel CL, et al. Efficacy and safety of trastuzumab as a single agent in first-line treatment of HER2-overexpressing metastatic breast cancer. J Clin Oncol. 2002; 20:719. [PubMed: 11821453]
27. Van Cutsem E, et al. Cetuximab and chemotherapy as initial treatment for metastatic colorectal cancer. N Engl J Med. 2009; 360:1408. [PubMed: 19339720]
28. Reichert JM, Dhimolea E. The future of antibodies as cancer drugs. Drug Discov Today. 2012; 17:954. [PubMed: 22561895]
29. Reichelt P, Schwarz C, Donzeau M. Single step protocol to purify recombinant proteins with low endotoxin contents. Protein Expr Purif. 2006; 46:483. [PubMed: 16290005]
30. van der Neut Kolfschoten M, et al. Anti-inflammatory activity of human IgG4 antibodies by dynamic Fab arm exchange. Science. 2007; 317:1554. [PubMed: 17872445]
31. Boder ET, Wittrup KD. Yeast surface display for screening combinatorial polypeptide libraries. Nat Biotechnol. 1997; 15:553. [PubMed: 9181578]
32. Wang Z, Mathias A, Stavrou S, Neville DM Jr. A new yeast display vector permitting free scFv amino termini can augment ligand binding affinities. Protein engineering, design & selection: PEDS. 2005; 18:337.
33. Otwinowski, Z.; Minor, W. Methods in Enzymology. In: Carter, CW., Jr; Sweet, RM., editors. Macromolecular Crystallography, part A. Vol. 276. Academic Press; New York: 1997. p. 307-326.
34. Adams PD, et al. PHENIX: a comprehensive Python-based system for macromolecular structure solution. Acta crystallographica Section D, Biological crystallography. 2010; 66:213.
35. Emsley P, Lohkamp B, Scott WG, Cowtan K. Features and development of Coot. Acta crystallographica Section D, Biological crystallography. 2010; 66:486.
36. Kohrt HE, et al. Stimulation of natural killer cells with a CD137-specific antibody enhances trastuzumab efficacy in xenotransplant models of breast cancer. J Clin Invest. 2012; 122:1066. [PubMed: 22326955]

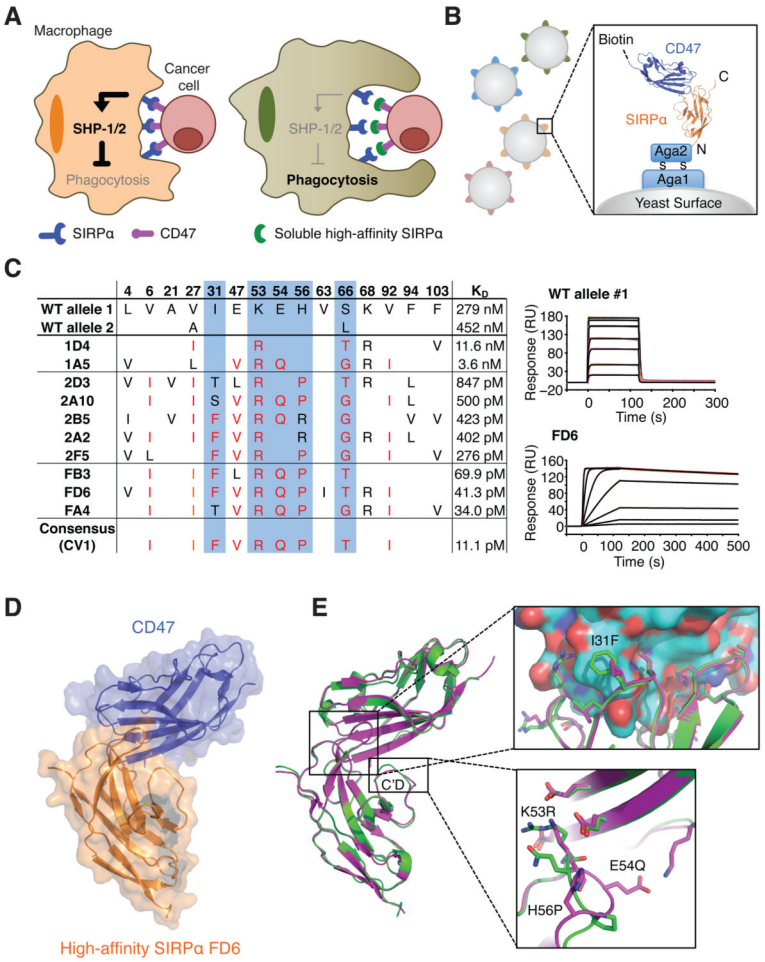

	4	6	21	27	31	47	53	54	56	63	66	68	92	94	103	K_D
WT allele 1	L	V	A	V	I	E	K	E	H	V	S	K	V	F	F	279 nM
WT allele 2				A							L					452 nM
1D4					I		R				T	R			V	11.6 nM
1A5	V			L		V	R	Q			G	R	I			3.6 nM
2D3	V	I	V	I	T	L	R		P		T	R		L		847 pM
2A10		I		I	S	V	R	Q	P		G		I	L		500 pM
2B5	I		V	I	F	V	R	Q	R		G			V	V	423 pM
2A2	V	I		I	F	V	R		R		G	R	I	L		402 pM
2F5	V	L			F	V	R		P		G		I		V	276 pM
FB3		I		I	F	L	R	Q	P		T					69.9 pM
FD6	V	I		I	F	V	R	Q	P	I	T	R	I			41.3 pM
FA4		I		I	T	V	R	Q	P		G	R	I		V	34.0 pM
Consensus (CV1)		I		I	F	V	R	Q	P		T		I			11.1 pM

Fig. 1. Directed evolution of high-affinity SIRPα variants

A Schematic of CD47 blockade by soluble high-affinity SIRPα. (Left) In the basal state, CD47 expression on cancer cells activates SIRPα on macrophages, initiating an inhibitory cascade through SHP 1 and 2 tyrosine phosphatases and preventing cancer cell phagocytosis. (Right) Soluble, high-affinity SIRPα protein competitively antagonizes CD47 and prevents engagement with SIRPα on macrophages, thereby disinhibiting phagocytosis. **B** Schematic representation of yeast surface-display of the human SIRPα V-set Ig domain (domain 1). Yeast clones (grey cells) present different variants of SIRPα (colored bumps). Inset indicates the linkage of SIRPα to the yeast cell surface via fusion with Aga2 and selection with biotinylated CD47. **C** Summary of sequences and SPR affinity measurements of engineered SIRPα variants. The position of the mutated residues and their corresponding sequence in wild-type allele 1 is denoted at the top of the table. Red text color indicates the consensus mutations and blue shading indicates contact residues in the consensus. Representative SPR sensorgrams of wild-type SIRPα and high-affinity variant FD6 binding immobilized CD47 are shown to the right. RU = response units. **D** The crystal structure of the FD6:CD47 complex depicted as transparent surfaces containing ribbon representations of FD6 (orange) and CD47 (blue). **E** Superimposition of the wild-type (magenta) and high-affinity (green) SIRPα:CD47 complexes. Insets show mutated contact residues in the SIRPα C′D loop (sticks) and the binding interface of CD47 (top, space fill; bottom, sticks).

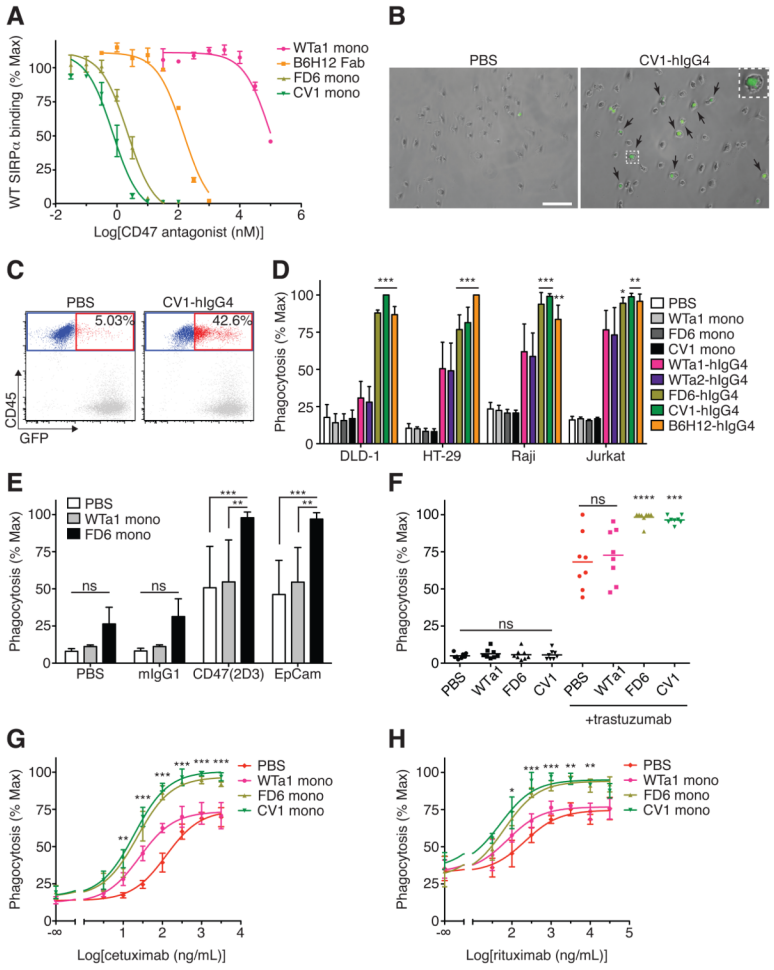

Fig. 2. High-affinity SIRPα variants lower the threshold for macrophage phagocytosis

A Dose-response curves of CD47 antagonism on Raji lymphoma cells with wild-type SIRPα allele 1 (WTa1, pink), anti-CD47 clone B6H12 Fab fragments (orange), or two high-affinity SIRPα variants as monomers (FD6, CV1, green). Cells stained with varying concentrations of CD47 blocking agents in competition with 100 nM Alexa Fluor 647-conjugated WT SIRPα tetramer. **B** Representative images of phagocytosis assays performed with GFP^+ DLD-1 colon cancer cells and primary human macrophages with vehicle control (PBS) or a high-affinity SIRPα variant fused to human IgG4 (CV1-hIgG4). Black arrows and inset show macrophages with ingested cancer cells. Scale bar = 100 μm. **C** Representative plots showing phagocytosis assays analyzed by flow cytometry. Phagocytosis was quantified as the percentage of macrophages (blue gate) that became GFP^+ (red gate). **D** Phagocytosis of GFP^+ tumor cells by donor-derived human macrophages as assessed by flow cytometry. All protein treatments used at 100 nM. **E** Phagocytosis of GFP^+ DLD-1 cells with vehicle, non-specific isotype control (mIgG1), non-blocking anti-CD47 (2D3), or anti-EpCam antibodies. All antibodies were used at 20 μg/mL. WTa1 SIRPα or high-affinity SIRPα variant FD6 monomers were combined as indicated. **F** Phagocytosis of GFP^+ SK-BR-3 breast cancer cells with vehicle, WTa1 SIRPα or high-affinity SIRPα monomers alone or in combination with 1 μg/mL trastuzumab. **G** Phagocytosis of GFP^+ DLD-1 cells with varying concentrations of cetuximab (anti-EGFR) alone (red) or in combination with WTa1 SIRPα monomer (pink) or high-affinity SIRPα monomers (green). **G** Phagocytosis of GFP^+ Raji cells with varying concentrations of rituximab (anti-CD20) alone (red) or in the presence of

WTa1 SIRPα monomer (pink) or high-affinity SIRPα monomers (green). **B-H** All human macrophage phagocytosis assays were performed with macrophages derived from a minimum of three independent blood donors. The percentage of GFP^+ macrophages was normalized to the maximal response by each donor for each cell line. Error bars indicate standard deviation. **E-H** All SIRPα variants were used at 1 μM. ns = not significant, *$p<0.05$, **$p<0.01$, ***$p<0.001$ versus WT SIRPα variants, or as indicated otherwise.

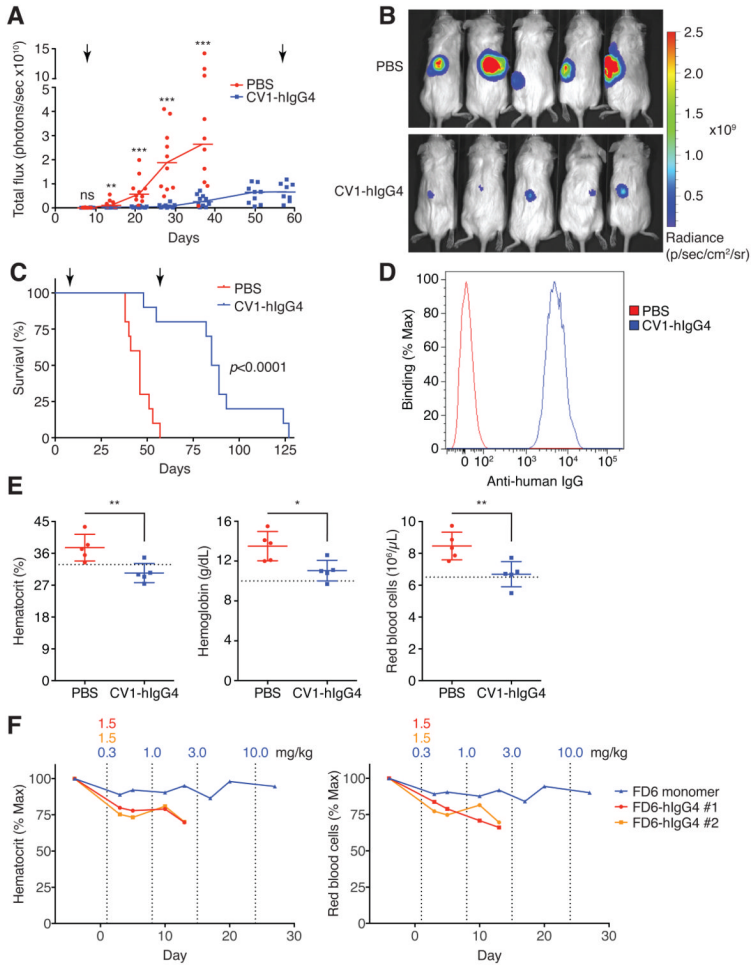

Fig. 3. High-affinity SIRPα-Fc fusion proteins are effective as single agents but produce toxicity

AGrowth of GFP-luciferase$^+$ 639-V bladder cancer cells in the dorsal subcutaneous tissue of NSG mice upon daily treatment with vehicle control (PBS) or high-affinity SIRPα-Fc (CV1-hIgG4) as evaluated by bioluminescence imaging. Bars indicate median values, points depict individual mice. Black arrows depict start and stop of treatment. **B** Representative bioluminescence images of 639-V-engrafted mice from each treatment group on day 37 post-engraftment. **C** Survival of mice engrafted with GFP-luciferase$^+$ 639-V cells. Black arrows indicate the start and stop of treatment. **D** Representative FACS analysis of human Fc bound to the surface of whole blood cells from treated animals. **E** Analysis of red blood cell parameters from treated animals showing mean and standard deviation from five animals per cohort. Dotted lines show lower limit of normal values. **F** Blood analysis of cynomolgus macaques treated with the indicated high-affinity SIRPα variants over time. Dotted lines indicate days of treatment with the doses indicated above in mg/kg. Data depicted as percentage of pre-treatment values. FD6-hIgG4 animal #2 was pre-treated with erythropoietin prior to toxicity testing. ns = not significant, *p<0.05, **p<0.01, ***p<0.001 for vehicle control versus CV1-hIgG4.

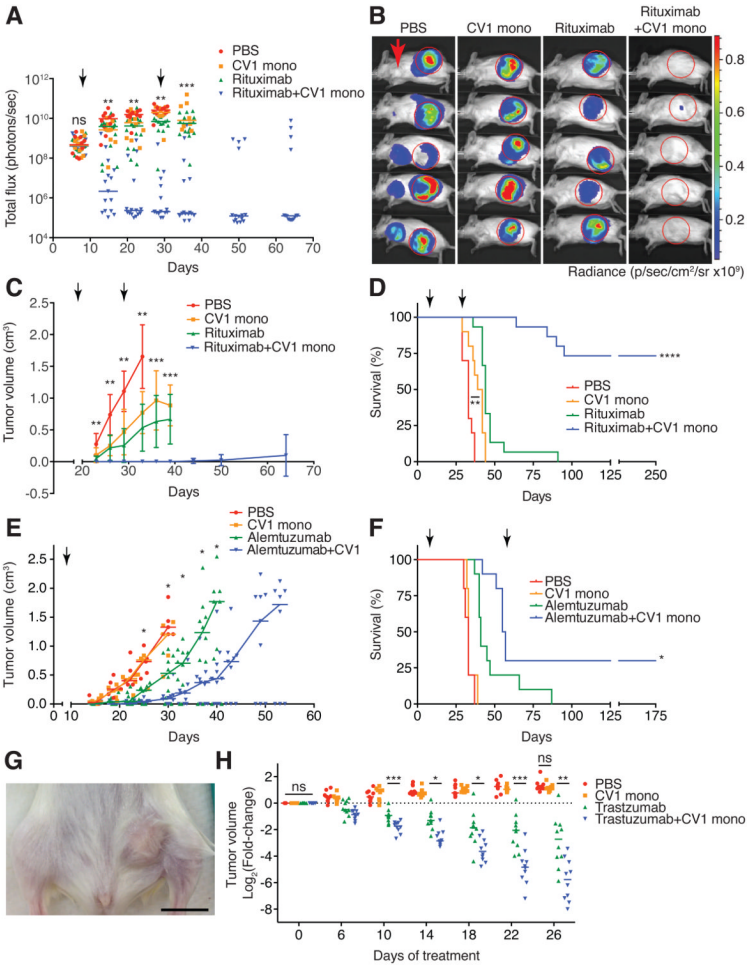

Fig. 4. High-affinity SIRPα monomers enhance the efficacy of therapeutic antibodies*in vivo*

A Growth of GFP-luciferase$^+$ Raji lymphoma tumors upon daily treatment with PBS (red), CV1 monomer (orange), rituximab (green), or rituximab plus CV1 monomer (blue), as evaluated by bioluminescence imaging. Bars indicate median values, points indicate values from individual mice. **B** Representative bioluminescence images of treated mice on day 29 post-engraftment. Red circles indicate sites of primary tumors, red arrow indicates site of metastases to axillary lymph nodes. **C** Mean tumor volume measurements of treated mice. Error bars depict standard deviation. **D** Survival of treated animals over time. **E** Growth of Raji lymphoma tumors upon biweekly treatment with PBS (red), CV1 monomer (orange), alemtuzumab (green), or alemtuzumab plus CV1 monomer (blue), as evaluated by tumor volume. Bars indicate median values, points indicate values from individual mice. **F** Survival of lymphoma-bearing mice from **E. G** Representative image of Her2/neu$^+$ BT474M1 human breast tumors engrafted into the mammary tissue of NSG mice prior to treatment. Scale bar represents approximately 1 cm. **H** Logarithmic fold-change in breast tumor volume upon treatment with the indicated therapeutic regimens. Bars indicate median values, points indicate values from individual mice. **A-F** Black arrows indicate the start and stop of the treatment period. ns = not significant, *p<0.05, **p<0.01, ***p<0.001, ****p<0.0001 for antibody alone versus antibody+CV1 monomer combination, or as indicated otherwise.